

**THE GENERATION OF A MATERIAL MODEL  
TO REPRESENT THE MECHANICAL BEHAVIOUR  
OF AN ALIPHATIC POLYETONE (CARILON EP)  
AT HIGH STRAIN RATE EVENTS  
AND LOW TEMPERATURES.**

*Dr. Jerome P J Coulton  
Advanced Car Technology Systems*

## Abstract

Although explicit finite element codes have been used for many years to predict the impact performance of plastic components, there are few papers that detail how the constants for material models were determined and the resulting models validated with experimental test results. Aliphatic polyetone materials appear very attractive materials for the developers of automotive fuel systems. This is principally due to their low fuel permeability and the stringent total vehicle evaporative requirements. This paper presents the analysis and results of the analysis of experimental test data to determine a material model for an aliphatic polyetone (Carilon EP) at high strain rates and low temperatures. Two different material models are compared (Johnson/Cook and Kruphowsky) with respect to their suitability to modelling Carilon EP and the chosen model validated with high speed impact tests.

## Introduction

The primary business of ACTS (Advanced Car Technology Systems) is the design and development of vehicle safety systems. During an accident the fuel system should remain sealed and not leak fuel. This is tested after an impact test with a static rollover procedure to ensure the leakage does not exceed the prescribed limits. In the process of developing a robust, durable vehicle fuel system, the crash worthiness of fuel system will normally be simulated using a finite element analysis simulation software such as LS-DYNA3D and PAMCRASH. Despite the fact that polymeric materials have been used for impact resistant applications for many years, the expertise to characterise the mechanical behaviour of these types of materials for use in the simulation of high strain rate events is not well developed [1]. The non-linear effects that occur in impact events may be broadly characterised as:

- 1) boundary (opening/closing of gaps, contact, follower force);
- 2) geometry - stress stiffening (membranes);
- 3) geometry - gross deformation with large rotations (snap through buckling);
- 4) geometry - large strains (engineering versus true stress and strain);
- 5) material - stiffness (plasticity, creep, viscoelasticity);
- 6) material - damage and failure (brittle, ductile).

Whereas the first four of these have been addressed in many commercial software analysis packages e.g. LS-DYNA3D and PAMCRASH, there are no universally accepted models for the strain rate dependent non-linear behaviour of thermoplastic materials [2]. A successful implementation of a material model is defined by:

- 1) its ability to simulate the tests whereby the material properties were determined;
- 2) its use to satisfactorily predict the performance of complicated three-dimensional objects.

In the case of most materials this means simulating the test whereby the true stress-strain curve was obtained. To determine adequacy of a three-dimensional structural prediction it is necessary to establish the sensitivity of the numerical prediction and the degree of correlation with experimental test results. Although there are various material models supplied with finite element analysis (e.g. LS-DYNA3D and PAMCRASH) the accompanying documentation does not detail how the user should determine appropriate material model constants.

In general the analysis of impact events applied to polymeric materials assume that the material properties are independent from the strain rate and the thermo-mechanical effects, which are known to occur. In Trantina & Nimmer's [3] approach it is suggested that a strain rate independent material stiffness can be used based on the maximum strain rate expected in the component. Despite reporting good results, it is known that this approach is limited and can result in wrong predictions [4]. It is also known that the accuracy of predictions is strongly dependent on the material model used [5].

In approaching the modelling of a polymeric material stiffness and failure the incorporation of non-linear effects must follow the logical sequence as dictated by the loading of a material from zero strain to failure. Thus the sequence of non-linear material effects that should be considered is:

- 1) strain rate/temperature dependent modulus;
- 2) nonlinearity of the stress-strain curve;
- 3) thermal softening;
- 4) damage and failure mechanisms.

## Material testing configurations

### The tensile test

A requirement of an analysis package, that can be used to simulate the impact performance of polymers, is that it uses the true stress and strain measures [6]. The reason for this is that to effectively use low modulus thermoplastics it is necessary to use the whole of the stress-strain curve by loading the material to strains at which the difference between engineering and true measures become significant. The simulation of the tensile test illustrates some of the competing deformation modes within polymers. It has been documented [3, 7] that there are two competing failure modes in polymers. These are described as shear yielding and crazing which infer that there should be a fundamental difference between tensile and compression yield of polymers. In the case of tensile loading existing voids may be encouraged to increase in size to form crazes whereas in the case of compressive loading these same voids are closed. This has been confirmed by experimental and theoretical studies [8]. During the tensile test the material softens i.e.  $d\sigma/d\epsilon$  decreases, up to the point of maximum test load, which is associated with shear yielding and ductile drawing. As the applied displacement increases the measured load decreases. Upon the formation of a stable neck in the tensile specimen and the response hardens i.e.  $d\sigma/d\epsilon$  increases, as the material crazes with polymers being drawn into a highly orientated state producing a fibrous material [9]. The use of bi-linear or creep models [10, 11], cannot predict the formation of necking and tri-linear [3] or other [12] material models have been proposed to model the unstable creation and subsequent stabilisation of the necking process. Whereas the tri-linear approach of Trantina & Nimmer [3] has successfully been used to investigate the localisation and formation of necks within the tensile test, Trantina & Nimmer's work has not embraced the questions of thermal softening and strain rate dependency.

### The Instrumented puncture test

Before considering the analysis of this configuration it is necessary to understand how the discs are tested and what measurements are made.

#### Test configuration

In general the disc will be impacted in a similar configuration to the British Standard 353B [13] and that the force time history trace of the piezo electric load cell will be compared with the predicted force between the hemispherical striker and the disc. Although it is assumed that the force recorded in the test is also that sustained by the specimen [14] this is not always true. The remotely measured response of the load cell is not necessarily that experienced by the specimen due to mechanical oscillations and wave propagation effects within the test apparatus. It is also important to note that the recorded response may be heavily filtered [14] by the physical characteristics of the measurement transducer, electronic circuitry and time domain aliasing. Hence experimental results can be very misleading [15]. If a well conditioned test is conducted, in which the transient dynamic effects of the impacting hemispherical striker and measurement load cell are minimal, then characteristics of the force time history can be attributed to a quasi static large deformation and contact problem [3, 15, 16] If the material has a strain rate dependent stiffness then the measured response is a function of incident energy and velocity [14]. Failure to include strain rate dependency of the material stiffness can result in poor correlation between test and analyses [17].

#### FE Analyses

Although finite element analyses have been carried out on the instrumented puncture test configuration [3, 15, 16, 17, 18] these have assumed that the materials have the following characteristics:

- 1) isotropic;
- 2) no dependence of behaviour on the hydrostatic component of stress;
- 3) identical yield behaviour in tension and compression;
- 4) no strain rate dependency or thermal effects;
- 5) material's one-dimensional stiffness can be defined by a bi-linear [16, 17] or tri-linear stress-strain curve idealisation.

Although the tri-linear elastic-plastic approach by Trantina & Nimmer [3, 15] appears to be successful, the analyses are "speculative" as the basis of their material model has not been rigorously proved, thus the good correlation may have been achieved by chance. In particular Trantina & Nimmer's approach of using the von Mises equivalent stress to define ductile failure has been proved wrong for modelling the impact response and ductile failure of strain rate dependent aluminium discs [19]. Although strain rate dependent material models which include thermo-mechanical effects have been proposed for the analysis of the instrumented puncture test [18], sufficient material data has not been collated to characterise the materials and they not been implemented in numerical analyses of complicated components. The use of an effective stress based failure criterion has been discounted as a suitable approach for modelling ductile [3, 16, 19] with the suggestion that failure modelling needs to be characterised by a fracture mechanics [16] or damage approach [19]. This is dramatically illustrated in Figure 1 which shows the effect of surface finish (and hence surface damage) on impact resistance.

## Attributes effects

From experimental studies an insight has been obtained into the mechanisms involved. The initial measured response is due to the hemispherical striker and the load cell responding as a single degree of freedom system. Damage initiates very early under the nose of the impacting striker [14, 20] this is localised [15] and progressive throughout the test [14]. The peak force is associated with the onset of specimen collapse and the penetration of the hemispherical striker [14]. Correlation of quasi-static analysis with test results indicate that the elastic response of the material accounts for little of the measured response [3] with the response being dominated by a small zone under the striker nose which is subject to very large strains. The stages of the predicted force time history are:

- 1) initial elastic response;
- 2) material yield under the nose of the striker and non-linear geometrical stiffening;
- 3) material softening and drawing under the nose of the striker;
- 4) rapid thinning and perforation of the disc.

These are indicated in Figure 1.

## Comparison of material models for use a finite element simulation

### Source of test data

The data used to generate the constants for the material models are given in reference [21]. MATLAB was used to extract the appropriate material constants from the test data using the “fmins” least squares equation fitting utility.

### LS-DYNA3D material model 15 - Johnson/Cook

The Johnson/Cook model is a strain rate and temperature sensitive elasto-plastic material with a power law hardening. It was selected as it is used for problems where strain rates vary over a large range and adiabatic temperature increases due to plastic heating cause material softening.

Johnson/Cook express the flow stress as:

$$\sigma_y = \left( A + B \bar{\epsilon}^{-p^n} \right) \left( 1 + c \ln \dot{\epsilon}^* \right) \left( 1 - T^{*m} \right)$$

where A, B, C, n and m = input constants

$\bar{\epsilon}^{-p}$  effective plastic strain

$$T^* = \text{homologous temperature} = \frac{T - T_{room}}{T_{melt} - T_{room}}$$

The material model can be considered as three parts.

- The first part  $\left( A + B \bar{\epsilon}^{-p^n} \right)$  defines the generic shape of the stress strain curve.
- The second part  $\left( 1 + c \ln \dot{\epsilon}^* \right)$  defines the strain rate sensitivity.
- The third part  $\left( 1 - T^{*m} \right)$  defines the thermal softening.

The values of the input constants for the material model were obtained by a partial differential equation approach. i.e. the input constants for the three parts of the material model were obtained separately, in sequence, holding the other parts of the material model constant.

At high strain rates the test duration is short (less than  $2^{1/2}$  seconds) and potential temperature rises do not have time to dissipate by radiation or conduction effects. As the temperature of the material is decreases its stiffness increases and hence the energy dissipated during plastic flow also increases. Experimental tensile test data indicated that are significant temperature rise in the material at high strain rates and low temperatures. This has also been documented for the Hopkinson pressure bar test [22].

The temperature rate parameter was extracted from the 10% flow stress measurements at various temperatures and strain rates (see Figure 2). Figure 3 shows the values for  $m$  calculated by keeping strain and strain rate constant the using the differences between adjacent flow stress measurements at different temperatures. As the thermal softening parameter is not calculated at one test temperature, but between test temperatures, an additional calculation was required. Assuming the thermal softening factor was independent of strain rate effects and using the high strain rate data (tests with duration less than 2\_ seconds), the average thermal softening parameter was calculated for the test temperatures. This is shown in Figure 4 and listed in Table 1.

The strain rate parameter was extracted from the 10% flow stress measurements at various temperatures and strain rates. Figure 5 shows the linear fits of the flow stress at constant temperature and strain with respect to the natural logarithm of the true strain rate. From the curve fits, shown in Figure 5, the strain rate parameter of the flow stress was obtained by dividing the gradient by the y-axis intersection. The strain rate parameter and its dependence on temperature is shown in Figure 6 and listed in Table 1.

The parameters for the shape of the stress/strain shape were extracted from the tensile test data at constant temperatures. The stress-strain tensile test data was normalised by dividing it by the strain rate factor and the thermal softening factor , using the constants in Table 1. For the thermal factor it was necessary to include an energy conversion factor. The specific energy and conversion into a temperature rise was calculated as follows. Above the yield point it was assumed that the all the mechanical energy was converted into heat. The values for the specific heat capacity used were are listed in Table 1. This normalised data was then fitted to the equation with the additional parameter  $E$ , the Elastic modulus. Figures 7, 8 and 9 show the curve fits of the data and the values of  $E$ ,  $A$ ,  $B$  and  $c$  are listed in Table 1.

The desired temperature for the material data was  $-40^{\circ}\text{C}$ . The interpolated data for this temperature was obtained by simple linear extrapolation of the values shown in italics in Table 1.

## LS-DYNA3D material model number 64 - power law hardening “Kruphowsky”

This is a strain rate sensitive elasto-plastic material with a power law hardening.

The material model follows the constitutive relationship of the form:

$$\sigma = k\varepsilon^m \dot{\varepsilon}^n$$

where  $k$ ,  $m$  and  $n$  = input constants.

The material model can be considered as two parts.

- The first part ( $k\varepsilon^m$ ) defines the generic shape of the stress strain curve.
- The second part ( $\dot{\varepsilon}^n$ ) defines the strain rate sensitivity.

The values of the input constants for the material model were obtained by a partial differential equation approach. i.e. the input constants for the two parts of the material model were obtained separately, in sequence, holding the other parts of the material model constant.

The strain rate parameter ( $n$ ) was extracted from the 10% flow stress measurements at various temperatures and strain rates. Figure 10 shows the fits of the natural logarithm of the flow stress at constant temperature and strain with respect to the natural logarithm of the true strain rate.

The strain rate parameter ( $n$ ) was extracted from the 10% flow stress measurements at various temperatures and strain rates. Figure 10 shows the fits of the natural logarithm of the flow stress at constant temperature and strain with respect to the natural logarithm of the true strain rate. From curve fits, shown in Figure 10, the strain rate parameter of the flow stress were from the gradient of the curve fits. The strain rate parameter and its dependence on temperature is shown in Figure 11 and listed in Table 2.

The parameters for the shape of the stress/strain shape were extracted from the tensile test data at constant temperatures. The tensile test data was divided by the strain rate factor . using the constants in Table 2, to normalise the data. This normalised data was then fitted to the equation with the additional parameter  $E$ , the Elastic modulus. Figures 12, 13 and 14 show the curve fits of the data and the values of  $E$ ,  $k$  and  $m$  are listed in Table 2.

The desired temperature for the material data was  $-40^{\circ}\text{C}$ . The data for this temperature was obtained by simple linear extrapolation of the values contained in Table 1 and the Johnson Cook model was used for the FEA simulations in this paper.

### Choice of material model

A simple comparison of Figures 7 to 9 with Figures 12 to 14 shows that the Johnson/Cook is a much better fit to the data than the Kruphowsky model.

## Simulation of the instrumented impact testing of disc samples

Two different test configurations were modelled: a simple supported sample and a clamped sample. These are shown in Figures 15 and 16. The strain rates in the disc impact test samples were 180 and 260 s<sup>-1</sup> for the simply supported and clamped configurations.

### Modelling assumptions

Initially 4 single integration point elements were used through the disc thickness. Single integration point elements were used due to the large strains. It was found that the number of elements, through the thickness, needed to be increased to circa 8 to successfully model the formation of the plastic neck.

### Friction

LS-DYNA3D uses a Coulomb friction model with the form:

$$\mu_C = \mu_D + (\mu_S - \mu_D)e^{-DC|v_{rel}|}$$

Where  $\mu_D$  is the dynamic coefficient of friction,  $\mu_S$  is the static coefficient of friction, DC is the exponential decay coefficient and  $v_{rel}$  is the relative velocity of the surfaces in contact.

No measurements of the clamping surface pressure and the coefficient of friction, between the jig and the test sample, were available. The static and dynamic coefficients of friction were obtained from the shell web page "<http://www.shellchemical.com/chemsite.nsf/Literature/SC:2157-95>" and the relevant parameters are listed in Table 4. The analyses assumed a clamping pressure (5 MPa). In the absence of other data the exponential decay coefficient was set at 0.1 to provide a smooth transient from the low static coefficient of friction to the high dynamic value. Figure 17 shows the effect of the exponential decay coefficient on the resulting friction coefficient. Also included is a coefficient of viscous friction (VC), which is used to limit the friction force to a maximum. The suggested value is the yield stress of the material in shear,  $VC = \frac{\sigma_0}{\sqrt{3}}$ . Where  $\sigma_0$  is the yield stress of the contacted material. For the material model 15, which has a variable yield stress, VC was set at  $\frac{A}{\sqrt{3}}$ .

In order to prevent undesirable oscillations in contact a damping coefficient (VDC), perpendicular to the contacting surfaces, was used. This was arbitrarily set at 25% of critical damping.

### Application of load

The application of load was based on observed test data. Samples of Carilon were tested in an ICI Instrumented Impact tester. During the impact tests the gas pressure of the machine was adjusted to achieve an approximately constant velocity. In practice the velocity increased slightly during the test. The variation in test velocity was an increase of approximately 5 to 6% compared to the average value during the contact and penetration phases of the test.

There were two parts of the simulation, which were prone to hour-glassing problems. These were the boundary supports and the dart point of contact. To prevent hour glassing at the support diameter, quadrature elements were used adjacent to the contact surfaces as the strains in these elements was below 40%. At the dart impact point a similar mesh density was used for the dart and disc.

To reduce CPU time the dart nose and clamping jig were modelled as rigid parts.

## Comparison of Measured and predicted impact responses

### Test results

The data that can be readily measured in disc impact tests is the low frequency responses of the load cell that the striker is mounted on and the displacement of the pneumatic ram. Only the low frequency response of the load cells can be used, as load cells are normally statically calibrated and not dynamically calibrated with the striker attached.

### Simply supported

The test samples were simply supported on a diameter of 50 mm in a steel jig and mounted in an ICI instrumented impact tester. A standard steel striker, with a 10 mm diameter hemispherical end, was used for the disc tests.

Four series of tests were undertaken for materials at different temperatures ( $-40^{\circ}$ ,  $-30^{\circ}$ ,  $-20^{\circ}$ ,  $+20^{\circ}$  C). For the sub-ambient tests the material samples were soaked in a thermal chamber for a minimum of 1 hour, after the temperature in the chamber had stabilised. For the tests the first half of the test samples for each material tested had one surface abraded using 150-grade abrasive paper. The second half of the samples were tested as moulded. All samples were tested in the same orientation, with respect to the injection-moulding tool, with the abraded samples being struck on the non-abraded face.

Before comparing the measured test and simulated disc impact responses it is important to understand that there are a variety of possible failure modes for a material. Figure 18 shows the results of impact tests for one batch of test samples at  $-40^{\circ}$  C. The test results depend upon moulding conditions and sample treatment (e.g. UV exposure, surface abrasion). The effect of sample treatment is shown in Table 5.

### Clamped

The test samples were clamped using diameter of 40 mm in an ICI instrumented impact tester. A standard steel striker, with a 10 mm diameter hemispherical end, was used for the disc tests.

Conclusion of the test results

The effect of temperature on the impact performance of Carilon is:

- Increased stiffness at low temperature
- Lower ductility at lower temperature
- **lower** strength at lower temperature
- **lower** energy absorbency at lower temperature
- Increasingly higher probability of **brittle failure** at low temperatures

### Test to Simulation comparison

For each of the two configurations the dart nose was driven into the Carilon sample using the test velocity profile. The resulting contact force between the test sample and the dart nose was compared with the measured load cell test data. Figures 19 and 20 show the comparison of the measured and predicted impact responses for the simply supported and clamped disc configurations. The tests were performed of two different batches of material. The initial batch of material was tested in a simply supported configuration and had a high probability of a brittle failure at sub-ambient temperatures. A second set of test was tests were undertaken with better results, however these also had a high probability of a brittle failure at sub-ambient temperatures.

The degree of correlation is remarkable especially considering that the test data, upon which the simulations based, is limited to 25% strain. In the clamped simulations the strains under the impactor exceeded 100%

In Figures 19 and 20 the following points of interest:

#### Simply supported disc

- Elastic limit/onset of plastic flow
- Onset of localised necking
- Brittle failure
- 
- 

#### Clamped disc

- Elastic limit/onset of plastic flow
- Onset of localised necking
- Collapse due to necking
- Ductile perforation of disc

### Sensitivity analysis

A sensitivity analysis was carried out using the two models (simply supported and clamped) to determine the parameters that have a critical effect on the measured test response. This was found to be the friction between the impacting dart and the test sample. In Figures 19 and 20 the dynamic coefficient of friction was changed from 0.49 to the static value of 0.07. For the brittle test sample tested in the simply supported configuration, Figure 19 does not show much difference in response between low or high values of friction coefficient. The more ductile clamped test samples however, showed that the friction coefficients had a significant effect on the measured force during the perforation of the disc (Figure 20). This effect is also reported elsewhere [17]. Due to its critical effect on the measured response, the modelling of friction between the impactor and the test sample requires further investigation.

### Ductile failure criterion/necking

The failure of a test sample due to the development of a neck in the instrumented disc impact test can be modelled as a thermally activated process with material model 15. The plastic deformation energy is assumed to be converted into a temperature rise. The temperature rise was calculated thus:  $\Delta T = \frac{1}{\rho C_p} \int \sigma \quad d\varepsilon_{PL}$  for the material coefficient fits using MATLAB. This temperature rise is assumed to soften the material until the melting temperature is reached when the material has zero effective stiffness. The rate of material softening is governed by the homologous temperature  $T^*$  and the softening coefficient  $m$ .

### Brittle failure criteria

A critical load limited brittle failure can be included in material model 15, as a critical cavitation pressure ( $p_{min}$ ). Figures 21 and 22 shown the development of cavitation pressure in the test samples during the impact simulations. It can be seen that the development of a necking zone under the impactor results in the pressure minima stabilising in the test sample this could account for the large scatter in the samples, which exhibited “brittle” failure. As brittle failure is initiated at the surface of the impacted test specimen, surface finish effects (e.g. abrasion) and the location of the element integration points relative to the elements surface have significant effect on the simulation results.

In predicting the impact failure of an engineering component the appropriate margins of safety need to be set. From the experience it is suggested that both minimum critical cavitation pressure and maximum plastic strain are used to determine the acceptability levels of stresses and strain. At present only an estimated failure criteria may be established. From the comparison of the experimental tests and the simulations thereof it is estimated that the first batch of material (simply supported) exhibited a high probability of failure at a cavitation pressure of circa –105 to –125 MPa and the second batch of material (clamped) exhibited a high probability of failure at a cavitation pressure of circa –110 to –125 MPa.

### Processing effects

Material processing can have a critical effect on the resulting strength of a component. E.g. injection moulding flow knit lines and the removal of runners and cutting of holes. These processing effects can sometimes have a greater effect on component performance than the accuracy of the material parameters in the impact simulation.

## Conclusions

1. The friction between the impacting dart and the test sample has a critical influence on the measured impact test sample response.
2. The model shows good correlation between the test and the analyses.
3. Failure defined by a loss of material stiffness, ductile necking, can be modelled as a thermally activated process.
4. The material tested exhibited a high probability of brittle failure when the cavitation pressure exceeded –105 to –110 MPa.

## References

1. J P J Coulton, "Effect of elevated strain rates on the mechanical behaviour of polyethylene structures", Ph.D. Thesis, University of Warwick, 1996.
2. J P J Coulton, "Non-linear design analysis of plastic fuel tanks", M.Sc. Thesis, University of Warwick, 1992.
3. G Trantina, R Nimmer, "Structural analysis of thermoplastic components" ,McGraw-Hill, 1994.
4. M A Wheel, "High speed double torsion testing of pipe grade polyethylenes", Ph.D. thesis Imperial College of Science and Technology, 1991.
5. H Kolsky, "The measurement of the material damping of high polymers over ten decades of frequency and its interpretation", ASTM Mechanics and mechanisms of material damping, publication 04-011690-23, pp.4-27, 1992.
6. D Hertema, "Property characterisation of PC/ABS blends for use in energy management applications", SAE paper 910402, 1991.
7. L E Nielson, R F Landel, "Mechanical properties of polymers and composites", Marcel Dekker, 1994.
8. C G'Sell, A Dahoun, M Aboulfaraj, "Modelling of the large-strain behaviour of amorphous and semi-crystalline polymers", POLYMAT '94, Imperial College London, pp. 244-227, 1994.
9. M E Vickers, H Fisher, "Real-time in-situ X-ray diffraction study of polyethylene deformation", Deformation yield and fracture of polymers, Churchill College, Cambridge University, April 1994.
10. B Harper, V Sura, "Non-linear thermoviscoelastic behaviour of thermoplastic films", Time dependent failure of polymers: Experimental study, ASME AMD Vol. 155, pp. 5-14, 1992.
11. P Krishnaswamy, M E Tuttle, A F Emery, "Finite element modelling of the time dependent behaviour of non-linear ductile polymers", Plastics and plastic composites: material properties, part performance and process simulation, ASME AMD Vol. 29, pp. 77-99, 1991.
12. M C Boyce E L Montagu, A S Argon, "The effect of thermomechanical coupling on the cold drawing process of glassy polymers", Plastics and plastic composites: material properties, part performance and process simulation, ASME AMD Vol. 29, pp. 47-75, 1991.
13. Anon., Method 353B Determination of multi-axial impact behaviour by the instrumented impact test, Methods for testing plastics. BS 2782 part 3.
14. P E Reed, "Developments in the instrumented impact testing of plastics and composites", Progress in Rubber and Plastics Technology, Vol 5 No. 2 pp. 157-172, RAPRA Technology Ltd.
15. L M Carapellucci, R P Nimmer, A F Yee, "Some problems associated with the puncture testing of plastics", Proceedings of the Society of Plastics Engineers Annual Technical Conference, ANTEC pp.622-628, 1986.
16. B A Crouch, "Numerical modelling of yield and fracture in plastics", Proceedings of the Society of Plastics Engineers Annual Technical Conference, ANTEC pp.1571-1573, 1986.
17. G Sala, M Angehileri, "Analytical and experimental evaluation of finite element models for crash analysis", Structures under shock and impact 2 - Proceedings of the 2nd International Conference, pp. 155-173, Portsmouth , June 1992.
18. Y Germain, J P Moulin, "Constitutive equations for polymer part design", POLYMAT '94, pp.426-429, Imperial College of Science and Technology, September 1994.
19. D J Bammann, M L Chiesa, A McDonald, W A Kawahara, J J Dike, V D Revelli, "Prediction of ductile failure in metal structures", ASME AMD Vol. 107 pp.7-12, November 1990.
20. C B Bucknall, "The relevance of impact testing in the materials science of polymers", Plastics rubber and composites processing and applications, Vol. 17 No. 3, pp.141-145, 1992.
21. P J de Vries P. J., "Mechanical behaviour of Shell CARILON EP", Interim graduation report, , Eindhoven Polymer Laboratories (EPL) Eindhoven University of Technology (TUE), 1997.
22. N N Dioh, "High strain rate behaviour of polymers at various temperatures", Ph.D. Thesis, Imperial College of Science Technology and Medicine, London, 1993.

# Figures

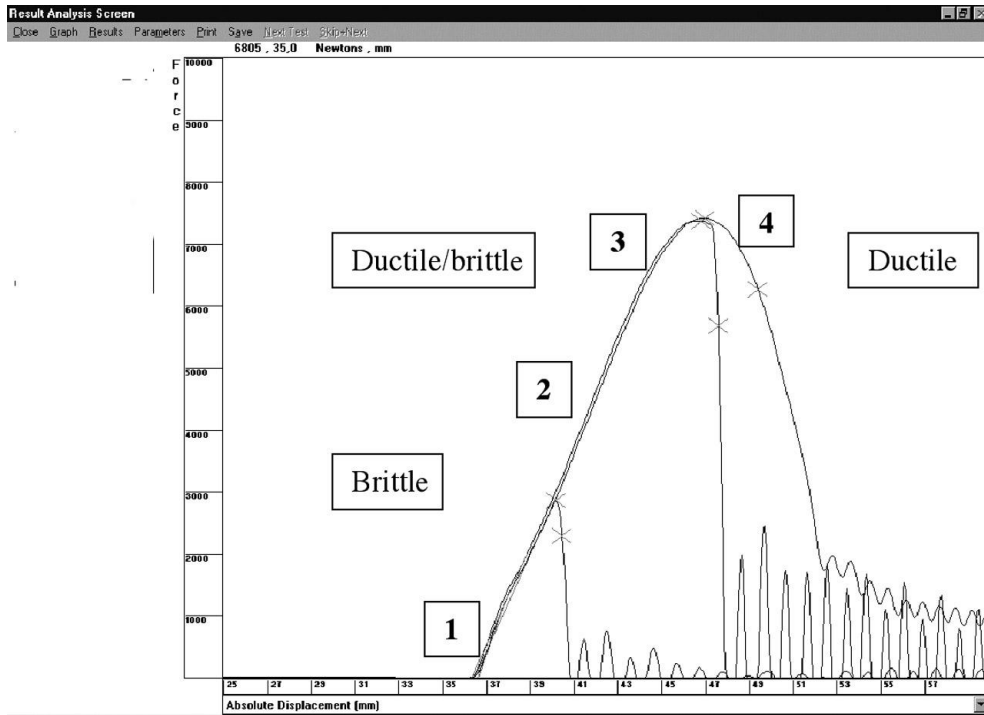


Figure 1 - Ductile/Brittle transition due to surface damage, Carilon EP  $-20^{\circ}\text{C}$

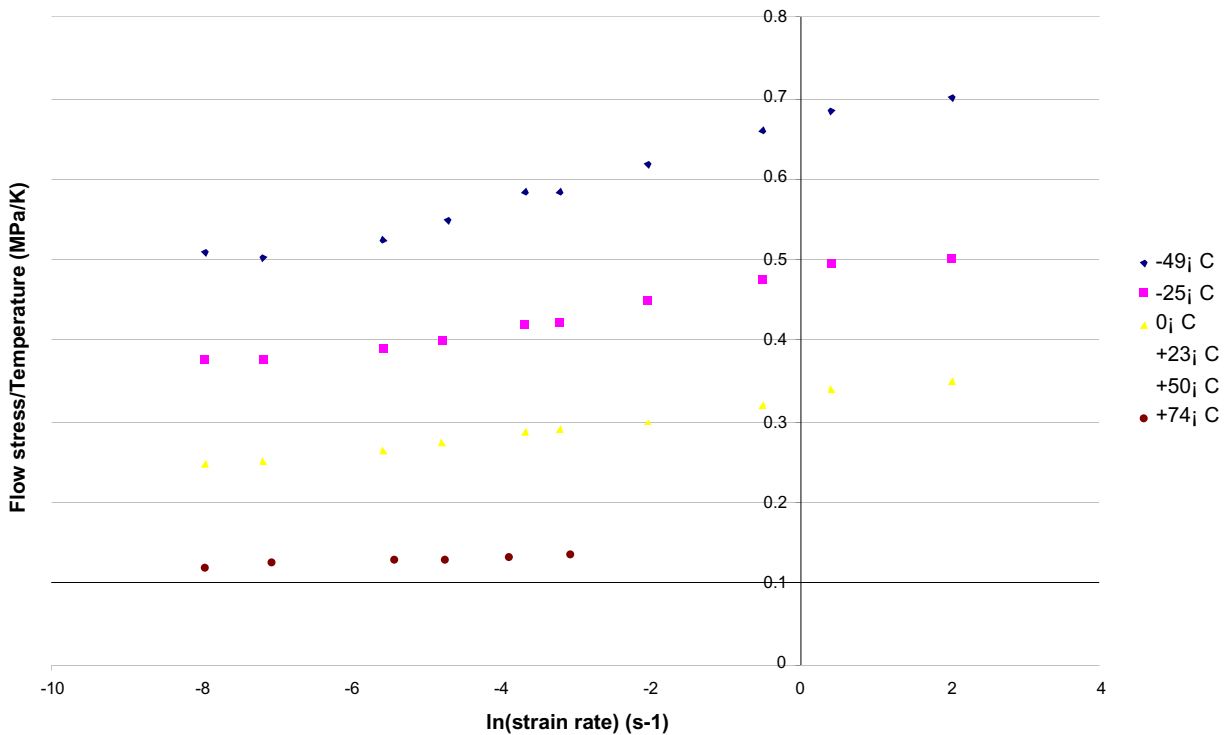


Figure 2 - Strain-rate dependence of 10% strain flow stress at various temperatures

Thermal softening parameter at 10% strain

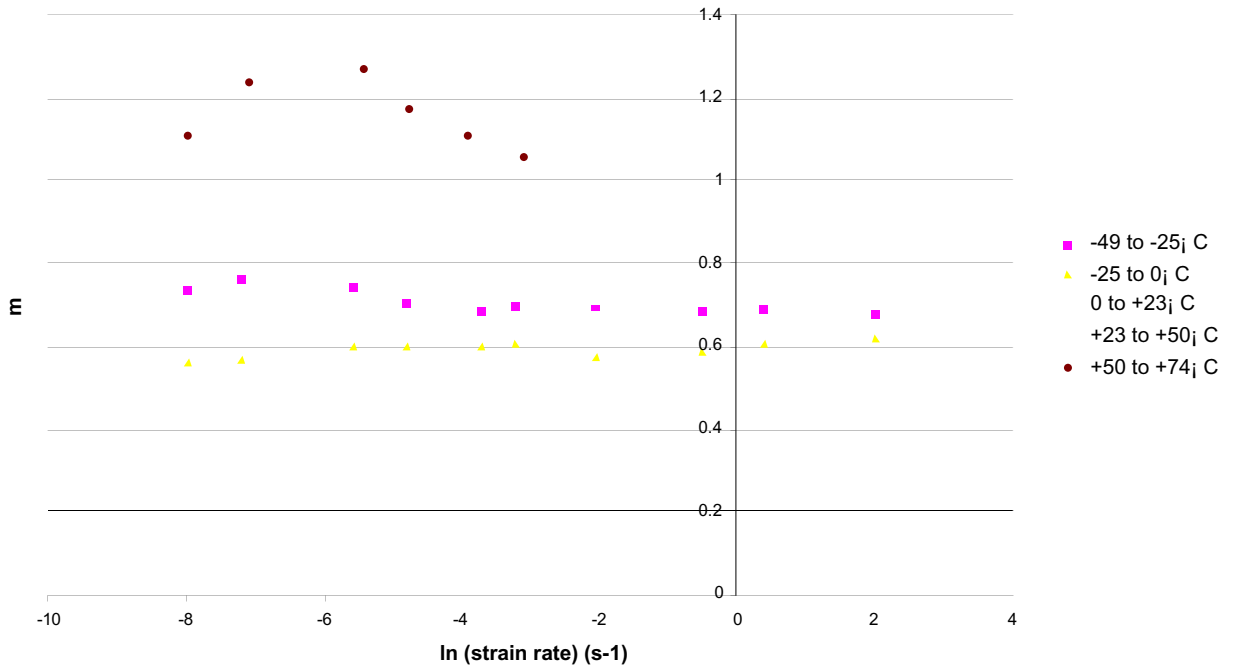


Figure 3 - JC - Temperature and strain rate dependence of thermal softening parameter (m)

Average thermal softening factor

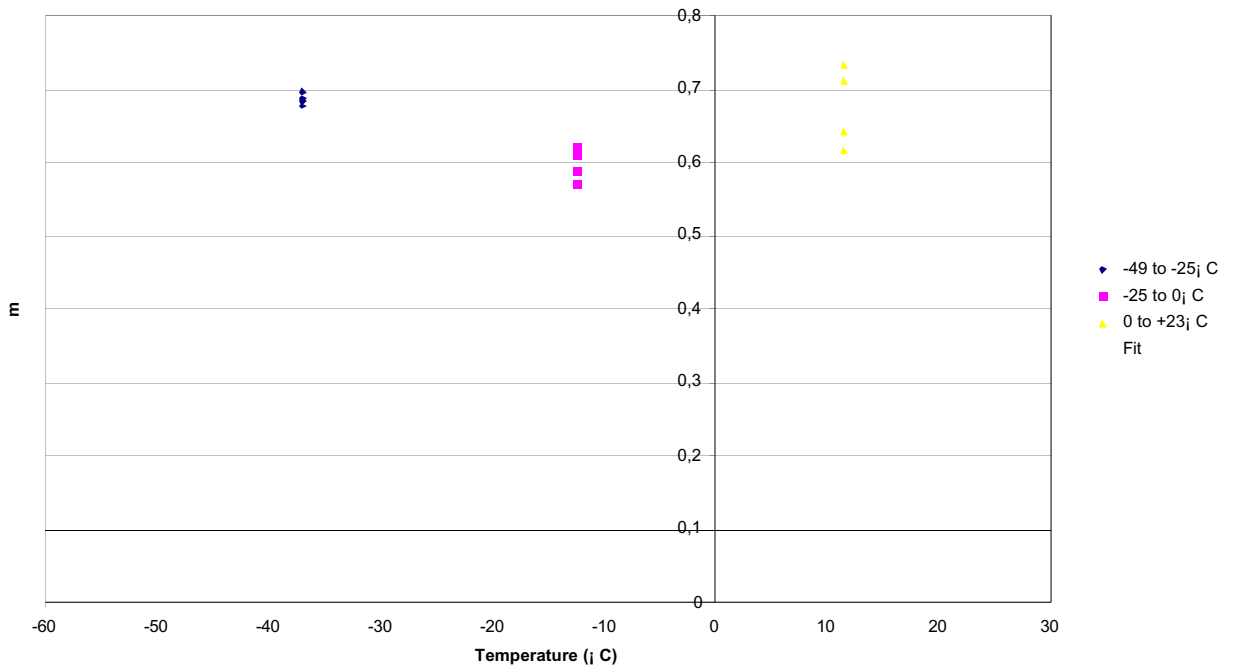


Figure 4 - JC - Average value for thermal softening parameter m

Flow stress at 10% true strain

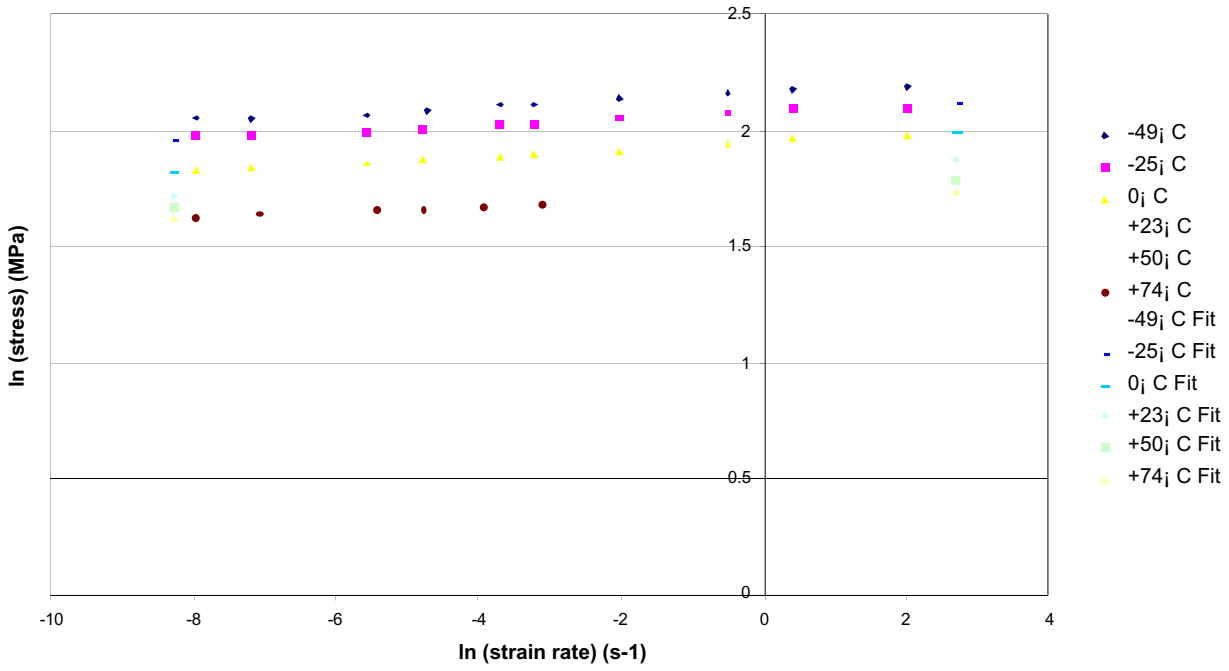


Figure 5 - JC - Flow stress data at 10% strain.

Strain rate parameter at 10% strain

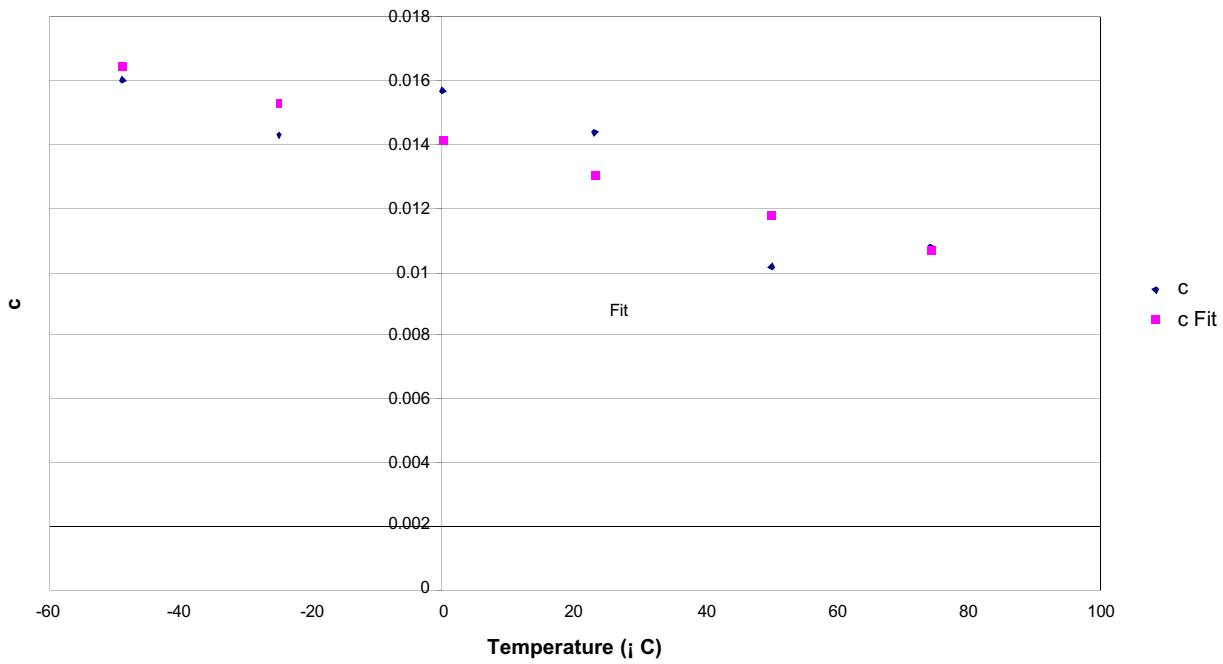


Figure 6 - JC - Effect of temperature on strain rate parameter

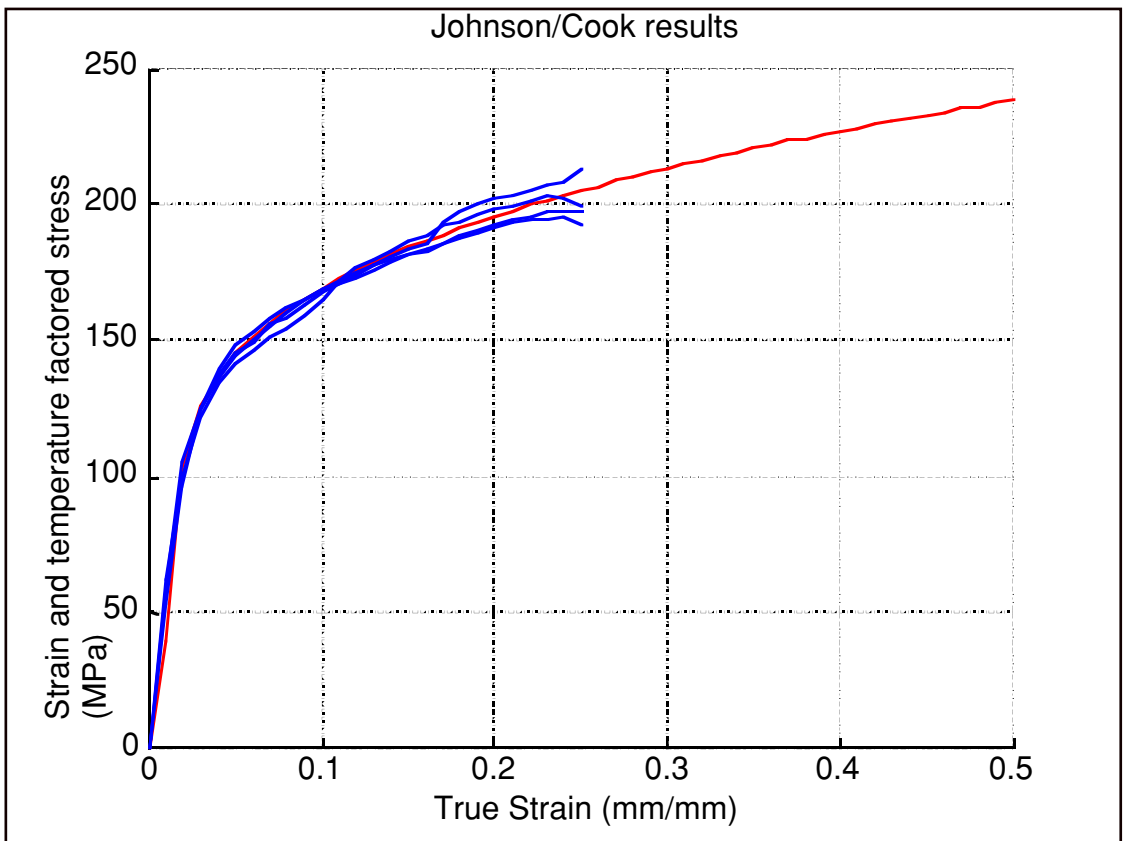


Figure 7 - JC - Curve fit at  $-49^{\circ}\text{C}$

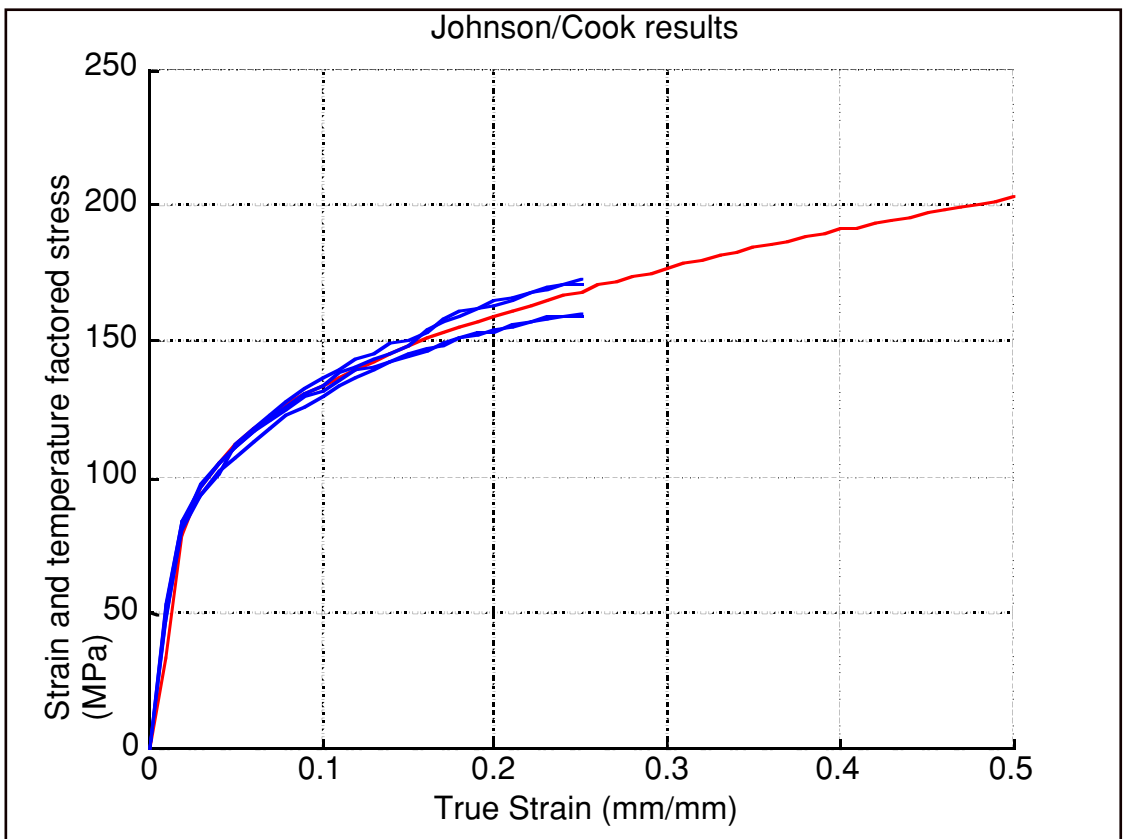


Figure 8 - JC - Curve fit at  $-25^{\circ}\text{C}$

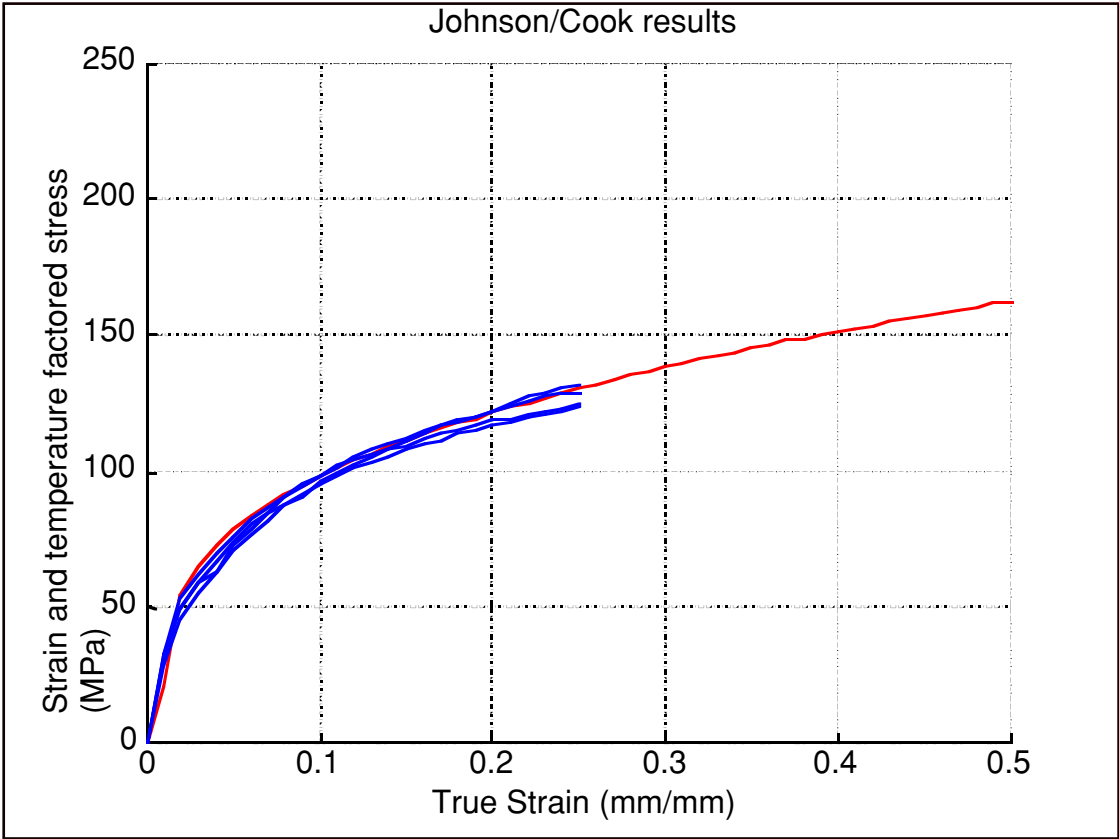


Figure 9 - JC - Curve fit at 0° C

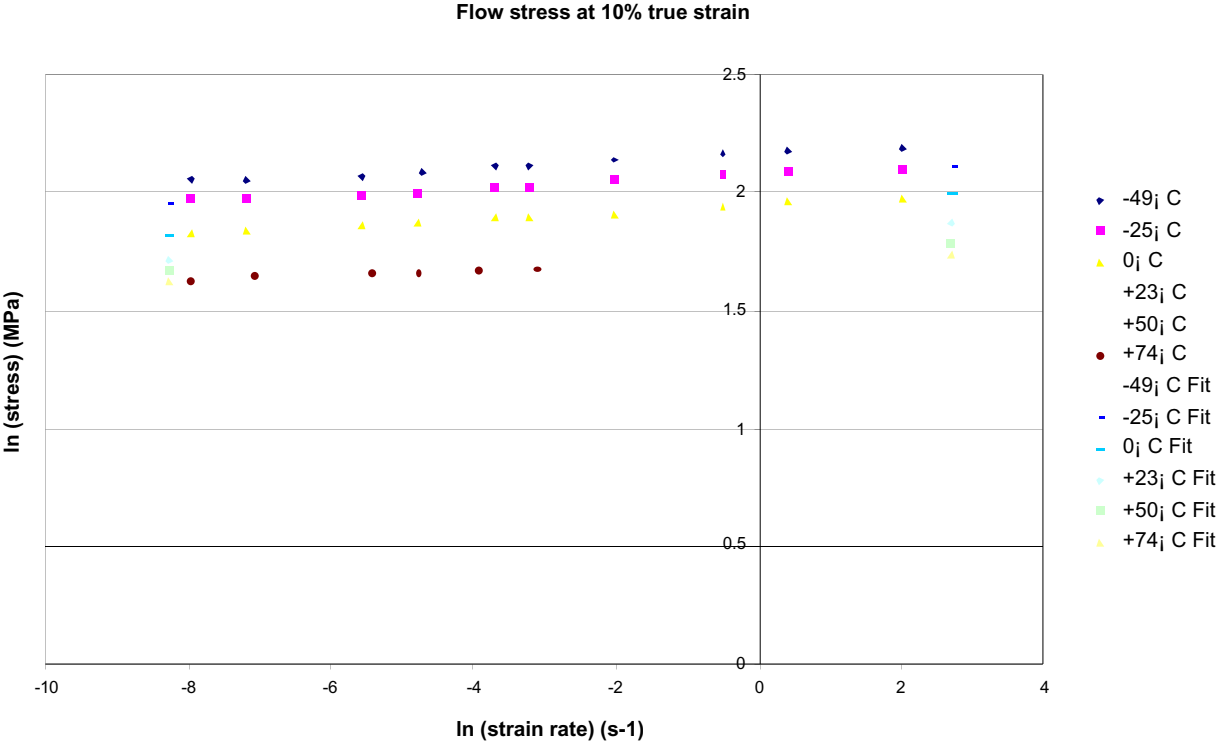


Figure 10 - K - Flow stress data at 10% strain.

Strain rate parameter at 10% strain

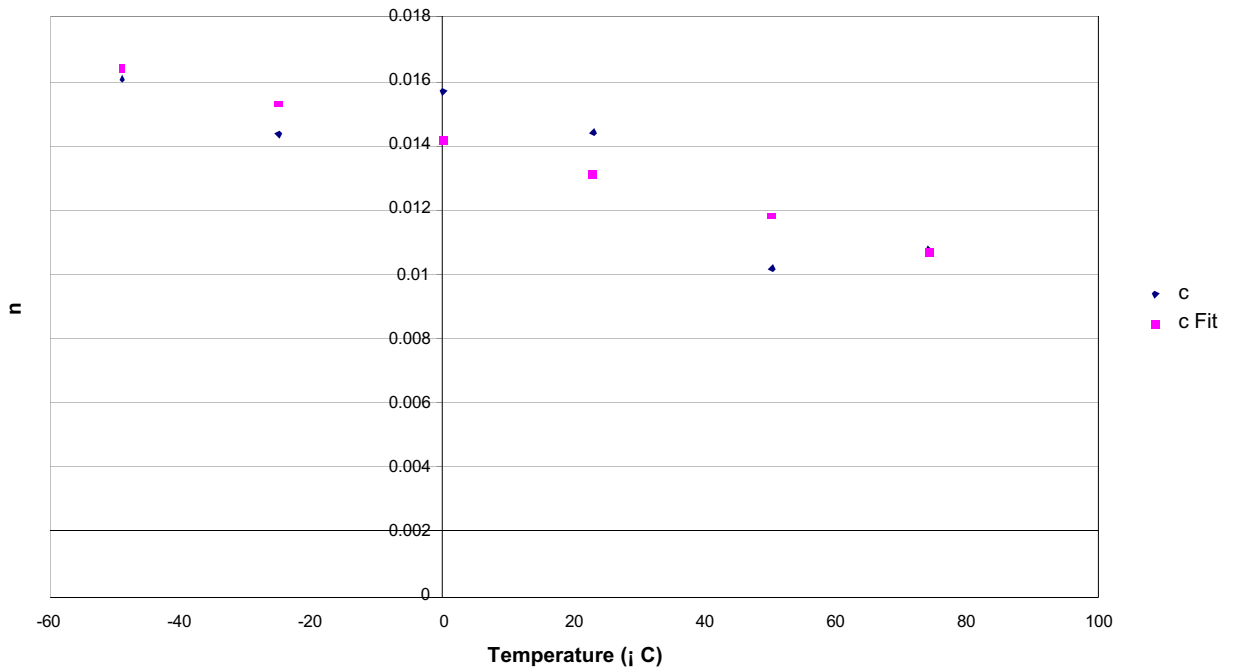


Figure 11 - K - Effect of temperature on strain rate parameter

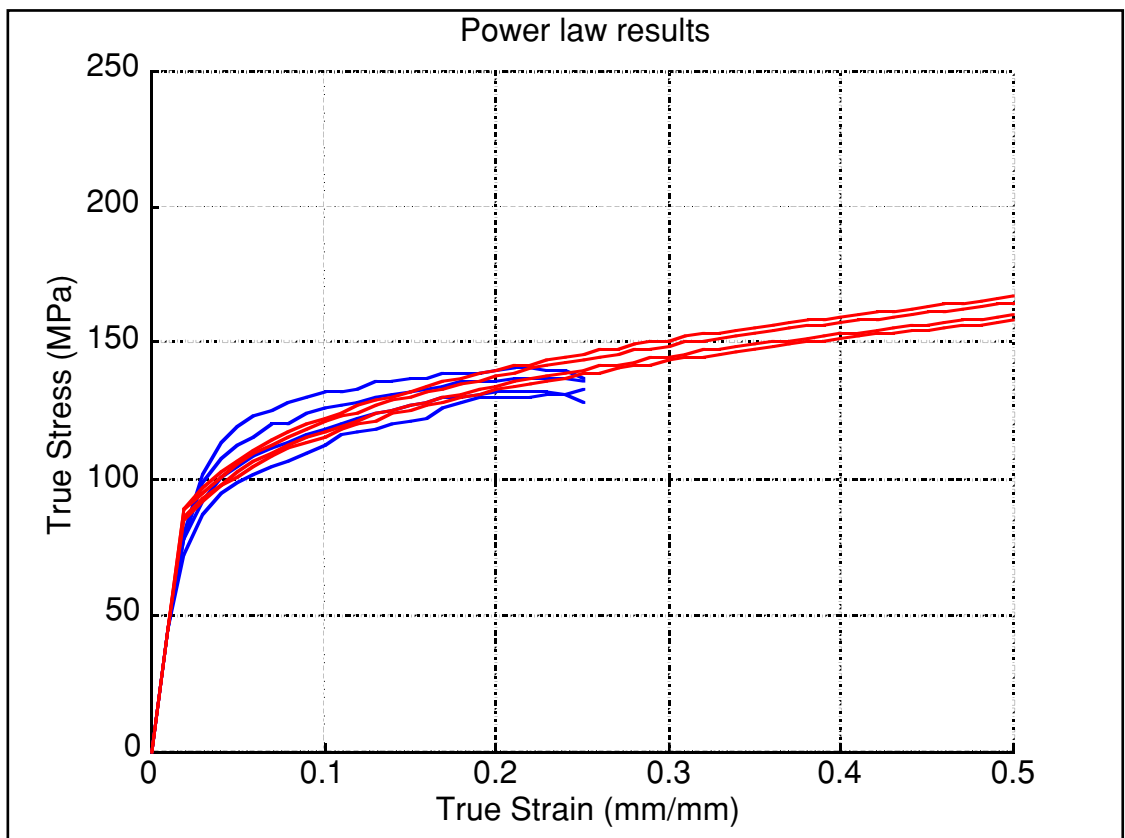


Figure 12 K - Curve fit at -49° C

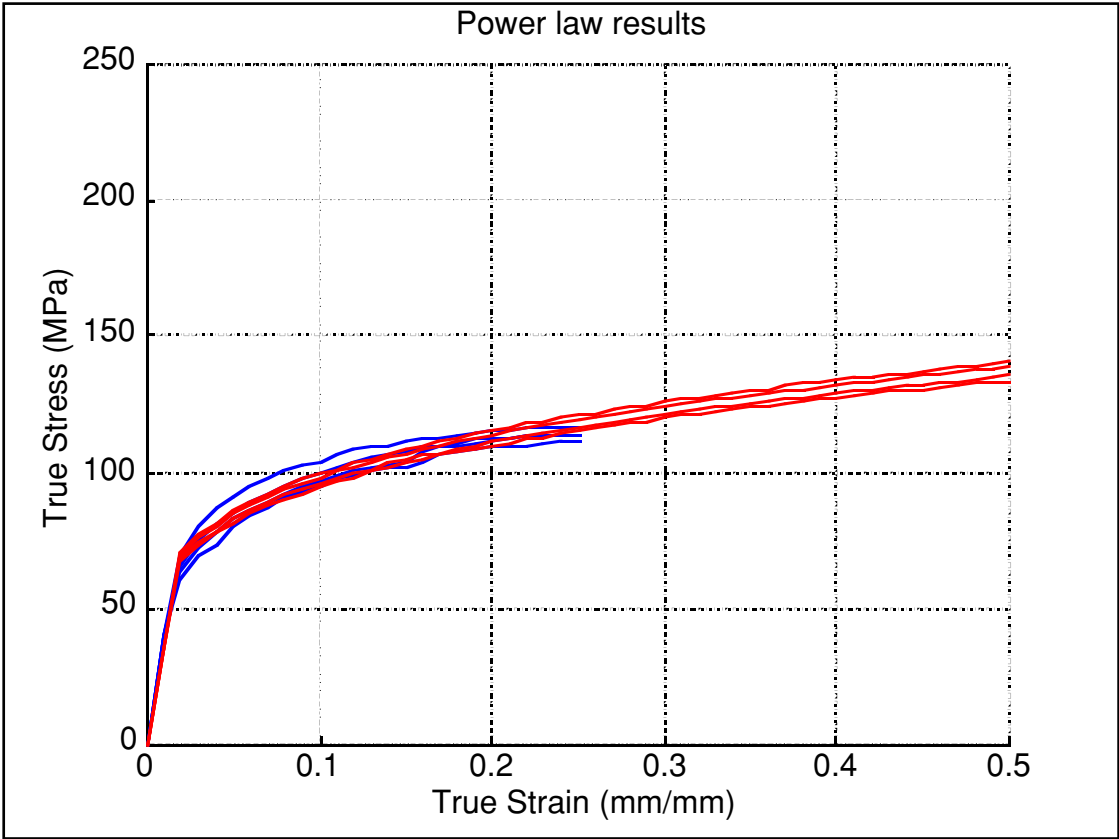


Figure 13 K - Curve fit at -25° C

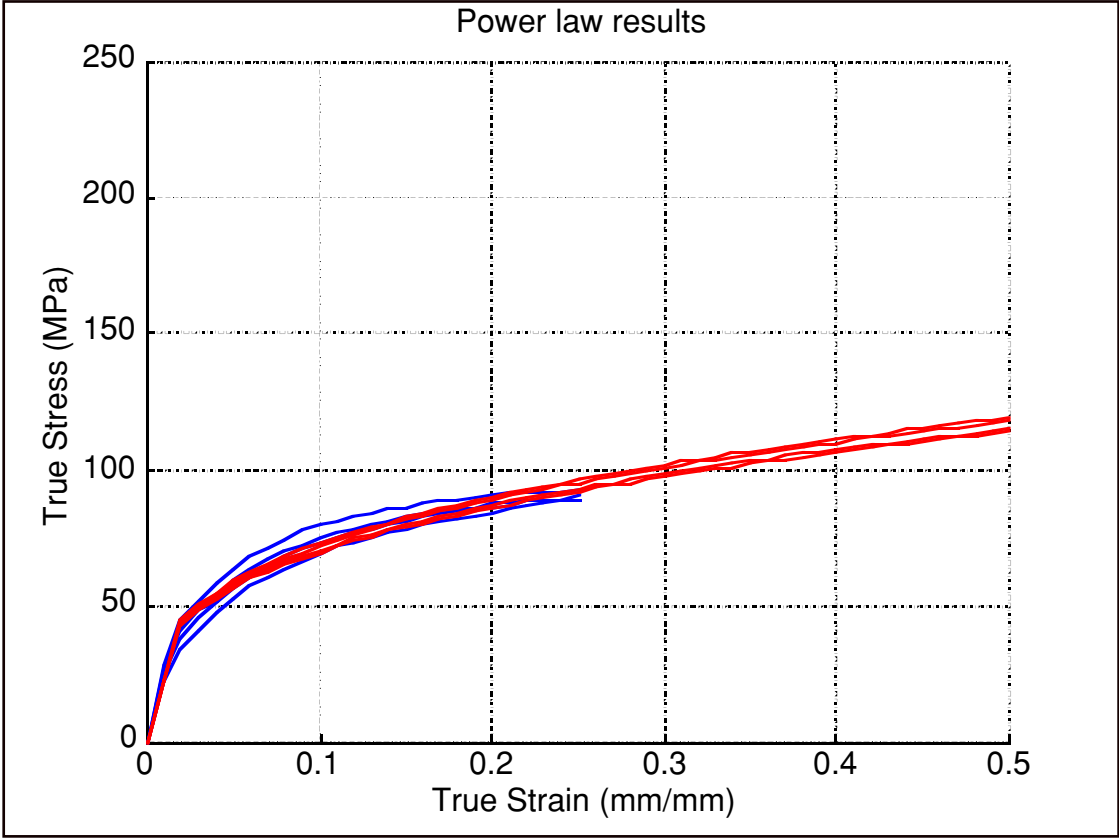


Figure 14 - K - Curve fit at 0° C

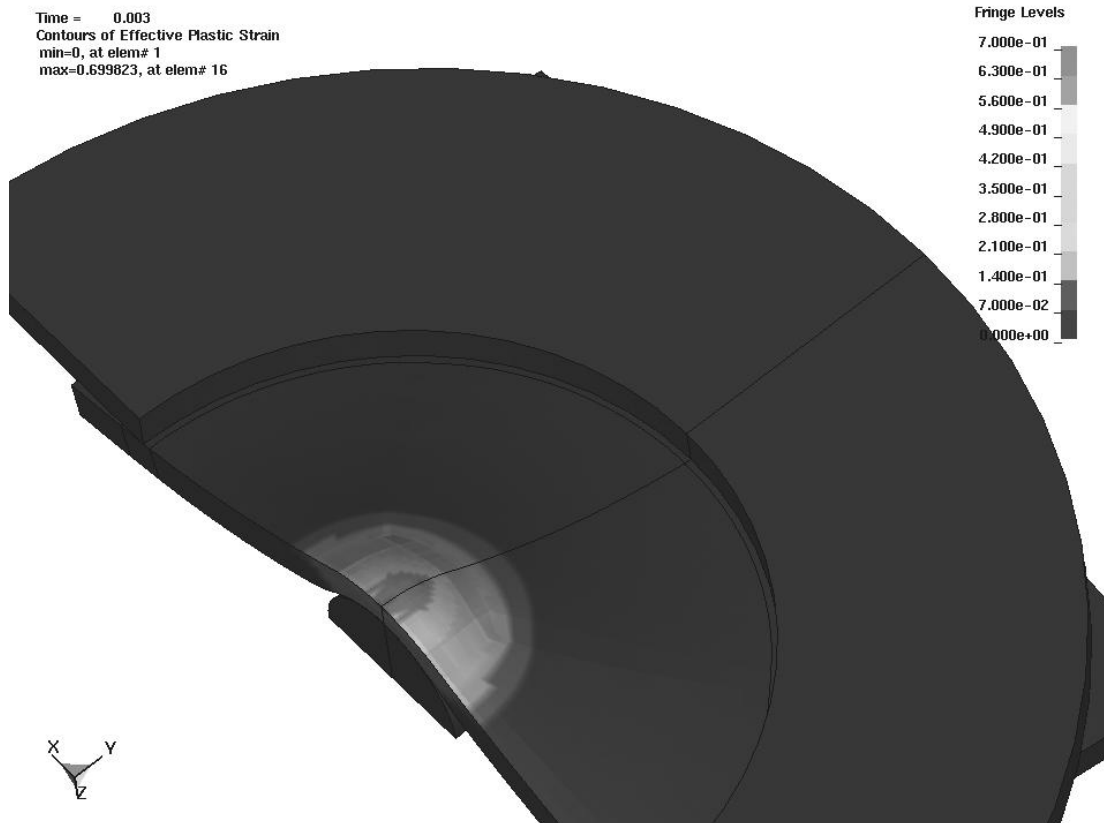


Figure 15 - Simply supported disc – Plastic strain

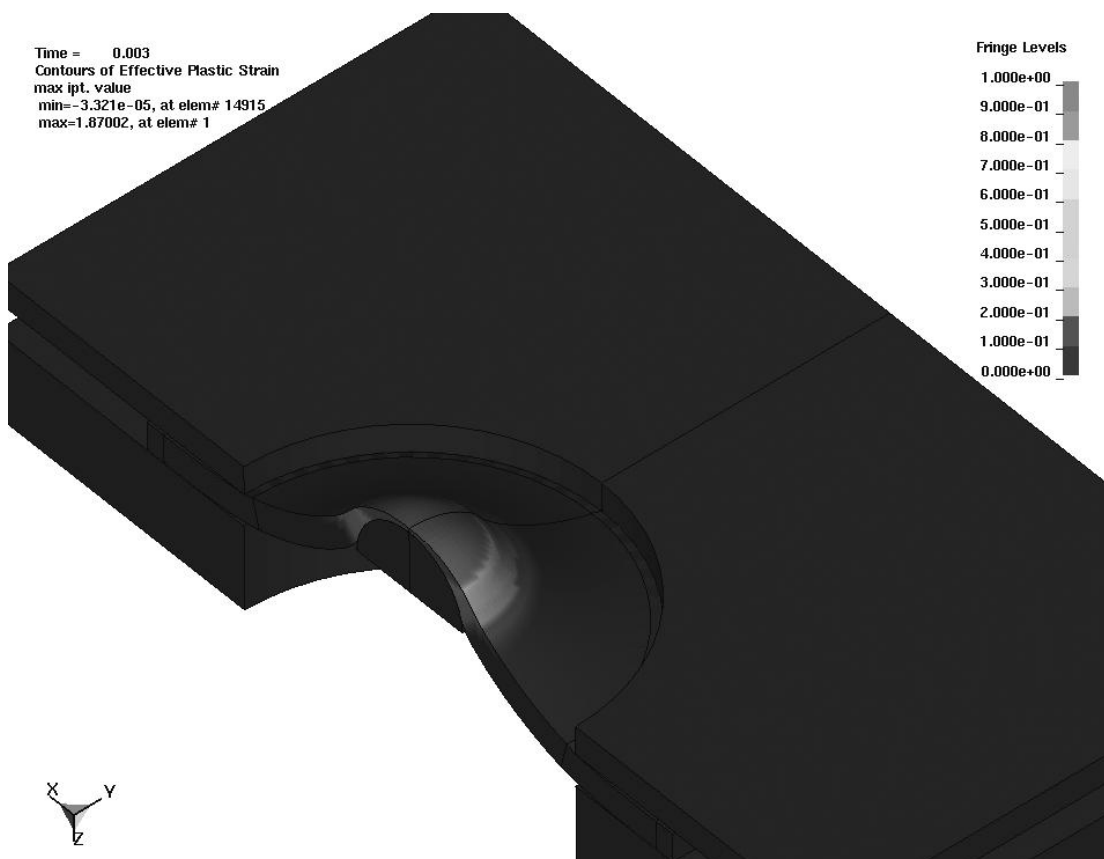
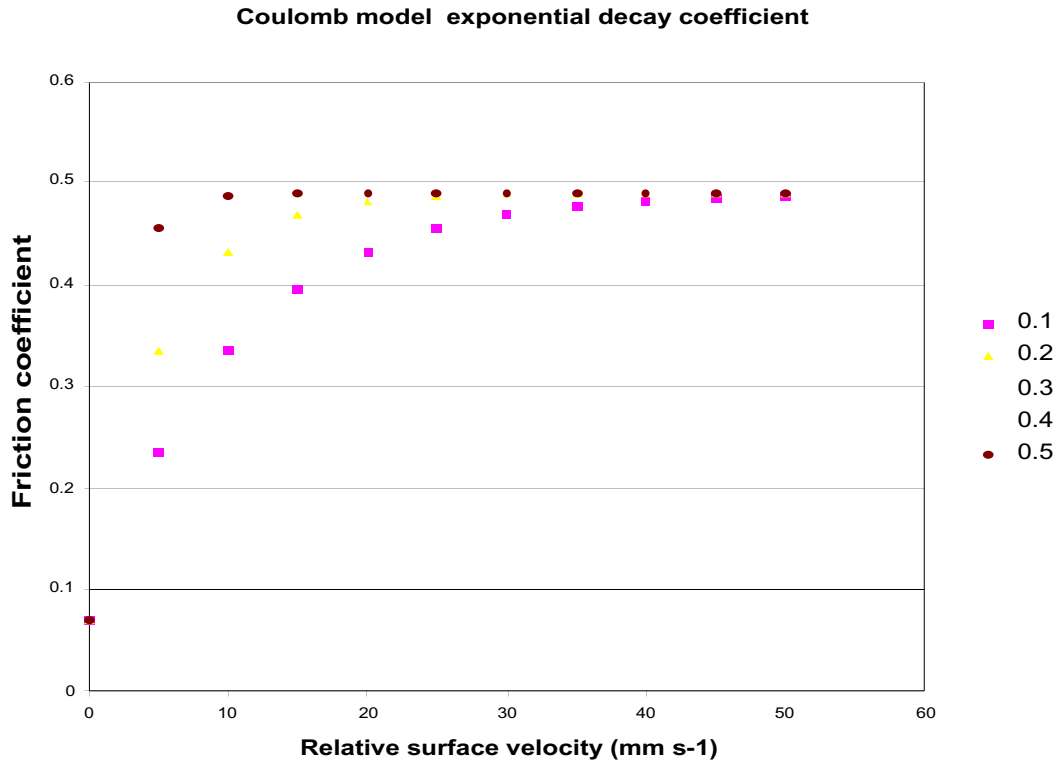
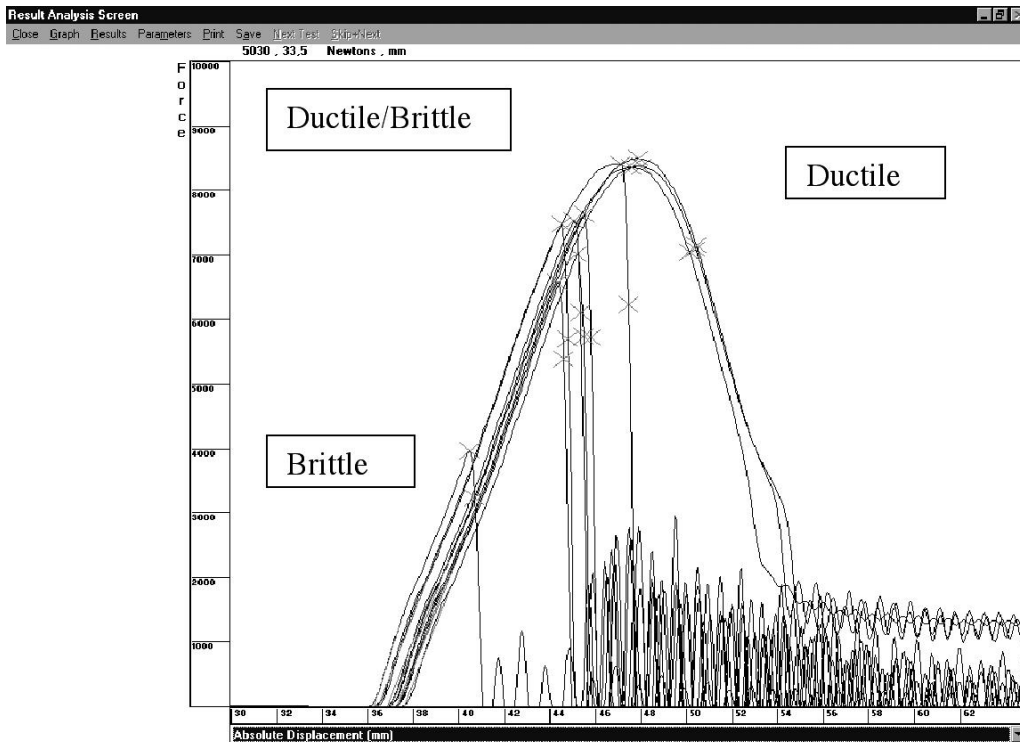


Figure 16 - Clamped disc – Plastic strain



**Figure 17 - Effect of changing the Friction model decay coefficient**



**Figure 18 - Test results at  $-40^{\circ}\text{C}$**

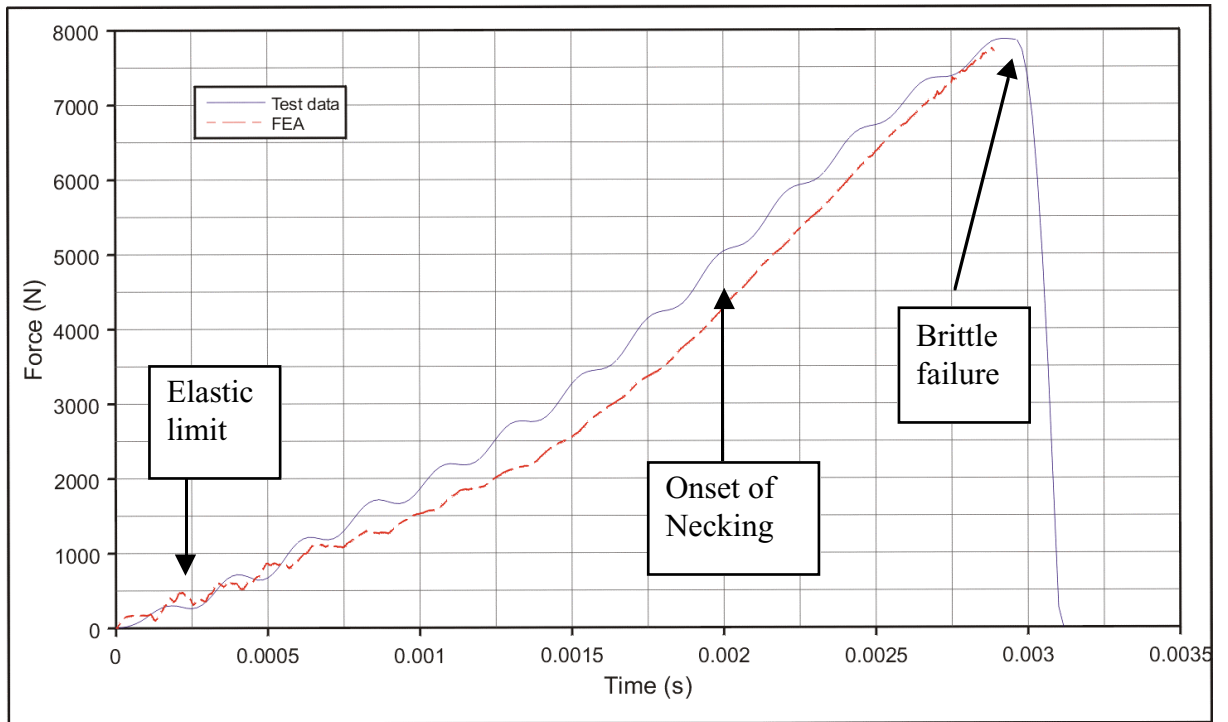


Figure 19 - Simply supported disc – comparison of measured and predicted forces

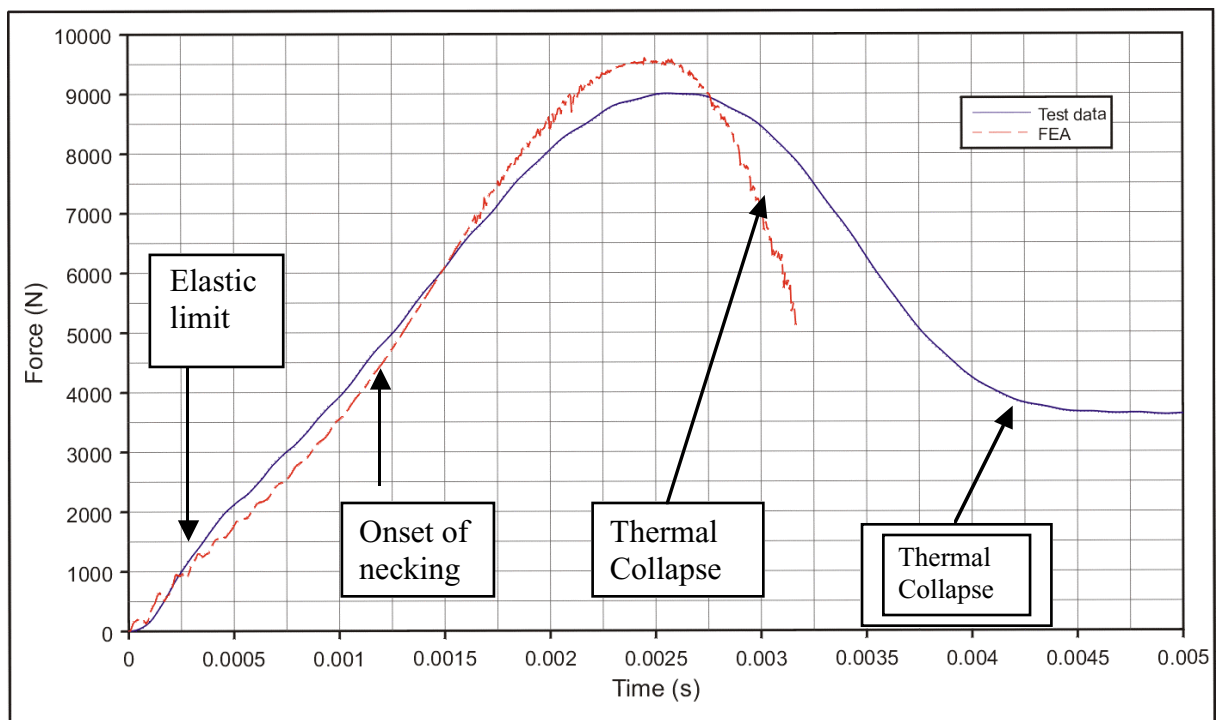


Figure 20 - Clamped disc – comparison of measured and predicted forces

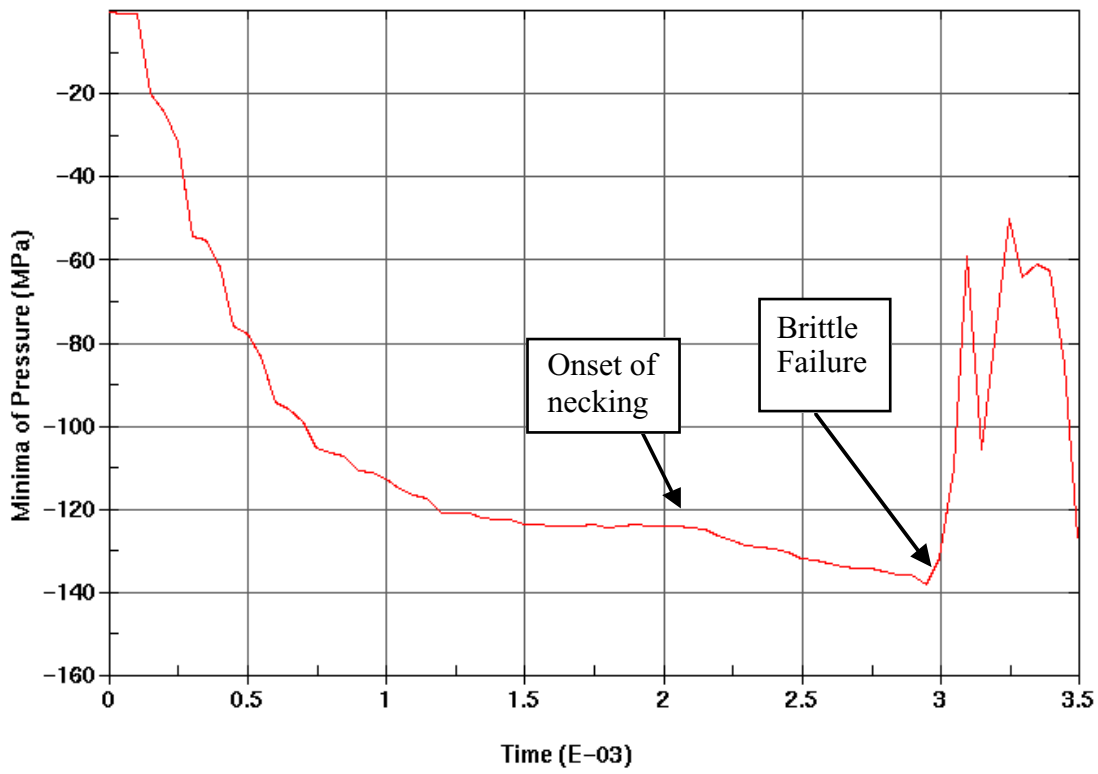


Figure 21 - Simply supported disc – Cavitation pressure

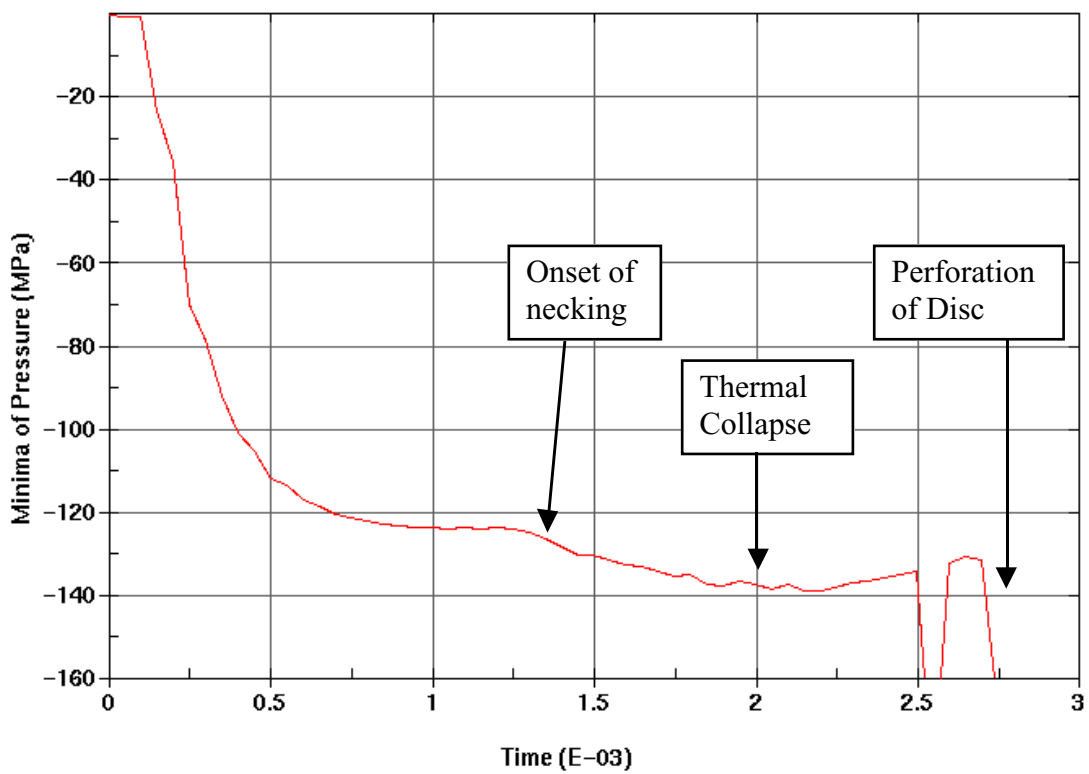


Figure 22 - Clamped disc – Cavitation pressure

## Tables

T (° C)	E (MPa)	A (MPa)	B (MPa)	n	c	m	Cp (J/KgK)	ρ (Kg/m <sup>3</sup> )
-49	3974	71.6	207.7	0.3101	0.0343	0.661	1605	1240
-40	3741	67.25	200.1	0.3336	0.0334	0.659	1612	1240
-25	3386	61.1	186.7	0.3759	0.0320	0.650	1622	1240
0	2090	27.8	177.3	0.3786	0.0295	0.655	1638	1240

**Table 1 - Johnson/Cook material data**

T (° C)	E (MPa)	k (MPa)	m	n	ρ (Kg/m <sup>3</sup> )
-49	4487	206	0.1927	0.0164	1240
-40	4120	194.8	0.2021	0.01602	1240
-25	3521	175.3	0.2144	0.0153	1240
0	2237	157.7	0.3049	0.0141	1240

**Table 2 - Kruphowsky material data**

Density	0.124E-08
Shear modulus	1.279E+03
Young's modulus	3.741E+03
Poisson's ratio	0.463000
A	6.725E+01
B	2.001E+02
N	3.336E-01
C	3.340E-02
M	0.659E+00
Melt temperature	493
Room temperature	233
Effective plastic strain rate	1.0
Specific heat	1.612E+09
Bulk modulus (C1 for EOS)	1.685E+04

**Table 3 - Johnson/Cook material data used in the simulations**

Parameter	Surface load		Relative surface velocity		Surface temperature		Coefficient of friction
	Psi	MPa	fpm	mm/s	°F	°C	
μS	25	0.172	-	-	0	0	0.07
μD	300	2.07	10	50.8	129	54	0.49

**Table 4 - Friction data for Carilon DP P1000**

	Temperature (° C)											
	-20°			-30°			-40°			-20°		
	D	D/B	B	D	D/B	B	D	D/B	B	D	D/B	B
Batch A – virgin	100	-	-	80	-	20	30	10	60	80	-	20
Batch A – abraded	30	10	60	-	30	70	-	-	100	20	30	50
Batch B – virgin	90	-	10	90	-	10	70	-	30	89	-	1
Batch B - abraded	30	30	40	20	50	30	-	-	100	33	11	56

**Table 5 - Summary of simply supported impact test failure modes**